Vol. 12 • No. 1 • January 2 • 2023

www.advhealthmat.de

# ADVANCED HEALTHCARE MATERIALS

WILEY VCH

ADVANCED HEALTHCARE MATERIALS
www.advhealthmat.de

# Assembly of Clay Nanotubes on Cotton Fibers Mediated by Biopolymer for Robust and High-Performance Hemostatic Dressing

*Yue Feng, Yunqing He, Xiaoying Lin, Mingyang Xie, Mingxian Liu,* and Yuri Lvov**

**Uncontrollable bleeding from military conflicts, accidents, and surgical procedures is a major life-threatening factor. Rapid, safe, and convenient hemostasis is critical to the survival of bleeding patients in prehospital care. However, the peel-off of hemostats such as kaolinite sheets from the cotton fibers often poses a risk of distal thrombosis. Here, an efficient clay hemostat of halloysite nanotubes is tightly bound onto commercial cotton fibers, which is capillary mediated by biopolymer alginate with $Ca^{2+}$ crosslinking. The robust clay nanotube dressing materials maintain high procoagulant activity after harsh water treatment, and only a few residuals of halloysite exist in the wound area. Compared with commercial hemostat QuikClot Combat gauze, halloysite-alginate-cotton composite dressing exhibits hemostatic properties both in vivo and in vitro with high safety. The hemostatic mechanism of the dressing is attributed to activating platelets, locally concentrating clotting components in the nanoclay, halloysite coagulation factors, and alginate cross-linked with $Ca^{2+}$. This work inspires robust self-assembly of clay nanotubes on textile fibers and offers a hemostatic material with balanced high hemostatic activity, minimal ingredient loss, and biocompatibility. The robust dressing based on halloysite tightly bounded cotton shows great potential for military, medical, and civil bleeding control with low health risks.**

## 1. Introduction

Death from acute hemorrhage is a tricky worldwide problem, since there is a lack of rapid and safe methods to control bleeding.[1] Most deaths can be avoided if emergency and effective measures are taken to stop the bleeding. Designing high-performance and safe hemostats always is a hot topic in academic research and industrial innovation. Among the different types of hemostatic materials, porous inorganic materials, including zeolite and kaolinite, have been widely developed due to their satisfactory blood coagulation properties.[2] For example, QuikClot combat gauze, approved by the U.S. Army, consists of a nonwoven material impregnated with kaolin.[3] However, the porous layered structure of the clays (including kaolin, montmorillonite, and halloysite) is highly hydrophilic and inevitably experiences severe shrinkage and swelling during the bleeding process.[4] This phenomenon severely reduces the mechanical strength and stability of the polymer fiber materials, causing clays on the fibers tend to fall off. As a result, the clay minerals enter into open wounds and follow the blood into the body, posing a potential risk of distal thrombosis and, in severe cases, amputation.[5] Hence, researchers have made many efforts to improve the robustness of hemostatic materials. QuikClot developed a clotting sponge based on zeolite (Encapsulates the particles in a sponge), which has been confirmed with life-saving properties under combat conditions in soldiers with uncontrolled bleeding. However, it is complex to handle, cannot be used for bandaging, and may cause wound burns due to the exotherm of zeolite.[6] In situ synthesis of Chabazite-type zeolites on cotton fibers is a good way to obtain robust dressing, but this method is not applicable to natural clay hemostatic materials.[4] Clay-based composites, including sponges,[7] hydrogels,[8] membranes,[9] etc., are designed with various functionalities, but they are either complex to prepare or expensive and inconvenient.[10] Alternatively, hemostatic particles are bonded to some polymer matrix with adhesives to achieve robustness, but this dilutes the active components and reduces its porosity, also resulting in potential toxicity brought by the adhesive.[11] To date, the ideal clay-based inorganic hemostatic material remains to be developed.

Previous studies have shown that halloysite clay nanotubes (HNTs), formed by rolling 20–30 layers of kaolin, have a superior hemostatic ability kaolin.[12] Multiple mechanisms were

Y. Feng, Y. He, X. Lin, M. Xie, M. Liu
Department of Materials Science and Engineering
College of Chemistry and Materials Science
Jinan University
Guangzhou 511443, P. R. China
E-mail: liumx@jnu.edu.cn
M. Liu
Engineering Research Center of Artificial Organs and Materials
Ministry of Education
Guangzhou 510632, P. R. China
Y. Lvov
Institute for Micromanufacturing, Louisiana Tech University
Ruston, LA 71272, USA
E-mail: ylvov@latech.edu

The ORCID identification number(s) for the author(s) of this article can be found under https://doi.org/10.1002/adhm.202202265

**DOI: 10.1002/adhm.202202265**

involved in the hemostatic process: i) rapid absorption of water by the capillary force of nanotubes to concentrate blood; ii) activating and promoting aggregation of platelets; iii) triggering of Factor XII and initiation of the coagulation cascade.[13] Moreover, due to their high biosafety, HNTs have been widely used in biomedical fields,[14] such as a nanocarrier to deliver drugs[15] and nucleic acids.[16] Studies found that smaller, looser clay particles exhibited an improved clotting effect due to high water absorption and activation capacity.[17] Compared with kaolin hemostats in Quik-Clot dressing, the size of HNTs is small, meanwhile HNTs have a unique hollow tubular structure with high aspect ratios. These structural differences produce a larger surface area, capillary effect, and water absorption ability. Taking dye adsorption studies as an example, HNTs exhibit higher adsorption capacity for both cationic and anionic dyes, roughly twice that of kaolin.[18] In addition, HNTs have an adequate divalent ion adsorption capacity due to their negative $SiO_2$ outer layer and positive $Al_2O_3$ inner layer.[19] More importantly, the tubular structure of HNTs forms an interconnected rigid porous network structure that can resist collapse and deformation compared to other laminated clays. The enhanced rheology property makes HNTs network more stable in liquid flow, such as blood flow.[20]

The interfacial self-assembly of nanoparticles has been a hot topic in advanced materials. The wetting-drying process was reported to mediate the self-assembly of HNTs on hair. When wetting, the squamous structure opens, and dispersed clay tubes penetrate it. Upon evaporation, the squamous structure closes, and the nanotubes form arrays anchored on the hair surface.[21] HNTs were loaded with selected dyes or drugs that allow hair coloring or medical treatment. Hydrophilic woven fibers such as cotton fibers, with their swelling (wetting)-contraction (drying) properties, are expected to be used as substrates for robust self-assembly.[22] However, the interfacial interactions between the functional nanoparticles and the fibers should be carefully designed. Previous studies reported that cellulose nanofibers could effectively tailor the assembled structure of carbon nanotubes, and anisotropic films can be formed from evaporation boundaries.[23] Algal polysaccharides could also cause liquid crystal phase during the evaporation of graphene dispersions, implying that the arrangement of the nanoparticles changed from isotropic to anisotropic.[24] Montmorillonite nanosheets (containing Al–OH) also can achieve constrained assembly by bridging hydrogen and ionic bonds with alginate and $Ca^{2+}$ ions.[25] Alginate also mediates capillary-driven self-assembly and enables the axial alignment of carbon nanotubes on cotton fibers, resulting in microstructure-dense nanotube arrangements. Then, $Ca^{2+}$ induced alginate cross-linking was used to improve the washing stability of the nanotube coating.[26] Carbon nanotubes can also be assembled on cellulose interfaces such as fabric and paper with the help of non-covalent interactions with sericin to increase water dispersion and stability.[27] $Ca^{2+}$ ion diffusion alone without using alginate could also direct the assembly of graphene oxide for thick multilayer coatings on arbitrary substrates.[28]

In this work, we systematically exploited the bonding interactions of HNTs with biopolymer alginate. A robust cotton dressing was then prepared by the in-situ assembly on the fiber surfaces driven by capillary and $Ca^{2+}$ ion binding. Interestingly, the assembled components involved in this HNT-alginate-cotton (called HAC) dressing all have synergistic hemostatic activity: i) HNTs are strongly procoagulant by multiple mechanisms; ii) $Ca^{2+}$ ions are cofactors of multiple coagulation factors,[29] and iii) alginate increases the aggregation of erythrocytes.[30] This rational design of dressing materials contributes significantly to the formation of local thrombus at the wound. It exhibits excellent clotting properties both in vitro and in vivo. In addition, HAC dressings have little residual on tissues and exhibit high biocompatibility toward cells and skin. The robust dressing can also maintain high procoagulant activity after washing. Consequently, the robust assembly of clay nanotubes on fibers provides a high-performance hemostatic material that balances procoagulant activity, active components loss, and biocompatibility for effective bleeding control.

## 2. Results and Discussion

### 2.1. Interactions between HNTs and Alginate and Their Potential for Ion-Driven Assembly

HNTs, with the chemical formula $Al_2Si_2O_5(OH)_4{\cdot}nH_2O$, are abundantly deposited in many countries and are cost-competitive (Figure S1a,b, Supporting Information). Before use, HNTs were purified by drying the upper dispersion after centrifuging of their aqueous dispersion at 4000 rpm (Figure S1c, Supporting Information). They have empty lumens, uniform size, and a high aspect ratio (Figure S1d–f, Supporting Information). The lengths range from 100 to 2000 nm with an average particle size of 313.7 nm (Figure S1i, Supporting Information), and their inner and outer diameters are 10–20 nm and 50–70 nm, respectively.[31] The surface area of HNTs is 67.4 $m^2\ g^{-1}$, larger than that of most clays such as kaolin (≈40.4 $m^2\ g^{-1}$),[32] which is attributed to the hollow tubular structure (Figure S2, Supporting Information).

In order to achieve a solid assembly on the fiber using capillary effect and ion diffusion, HNTs are bridged to alginate molecules via hydrogen bonding and to $Ca^{2+}$ on the fibers via ionic bonding, forming a nanotube-natural polymer network on the fiber matrix by evaporation (**Figure 1**a). The Fourier transform infrared (FTIR) spectra (Figure 1b, Figure S1d, Supporting Information) identifies the presence of Al–OH (3701 and 3626 $cm^{-1}$) and Si–O–Si groups (1006 $cm^{-1}$) on the surfaces. Alginate, a highly biocompatible natural polymer, is a good hydrogen bonding donor for clay nanotubes due to its rich content of oxygen-containing polar groups (–OH, –COO–, C–O–C), which can produce hydrogen bonding interactions with the inner lumen and outer surfaces of HNTs (Figure 1b). $Ca^{2+}$ is chosen because it is a potent ionic bonding agent for clay sheets and alginate molecules (Figure 1c,d).[25] Also, $Ca^{2+}$ plays an essential role in the tight regulation of the coagulation cascade, including coagulation factor X activation and the transition from prothrombin to thrombin.[33]

With the increased alginate amount, HNTs aqueous dispersion droplets show enhanced liquid crystals phenomenon in evaporation-mediated "coffee ring" formation (Figure 1e and Figure S3, Supporting Information), since a colorful texture structure appears in the HNTs-alginate group. This exciting finding indicates that the rod-like nanoparticles shift from isotropic to anisotropic upon drying, implying that the tubes are oriented in a particular direction via alginate mediation.[34] The X-ray photoelectron spectroscopy (XPS) wide-scan spectra (Figure S4, Supporting Information) of HNT-alginate and HNTs display the

 

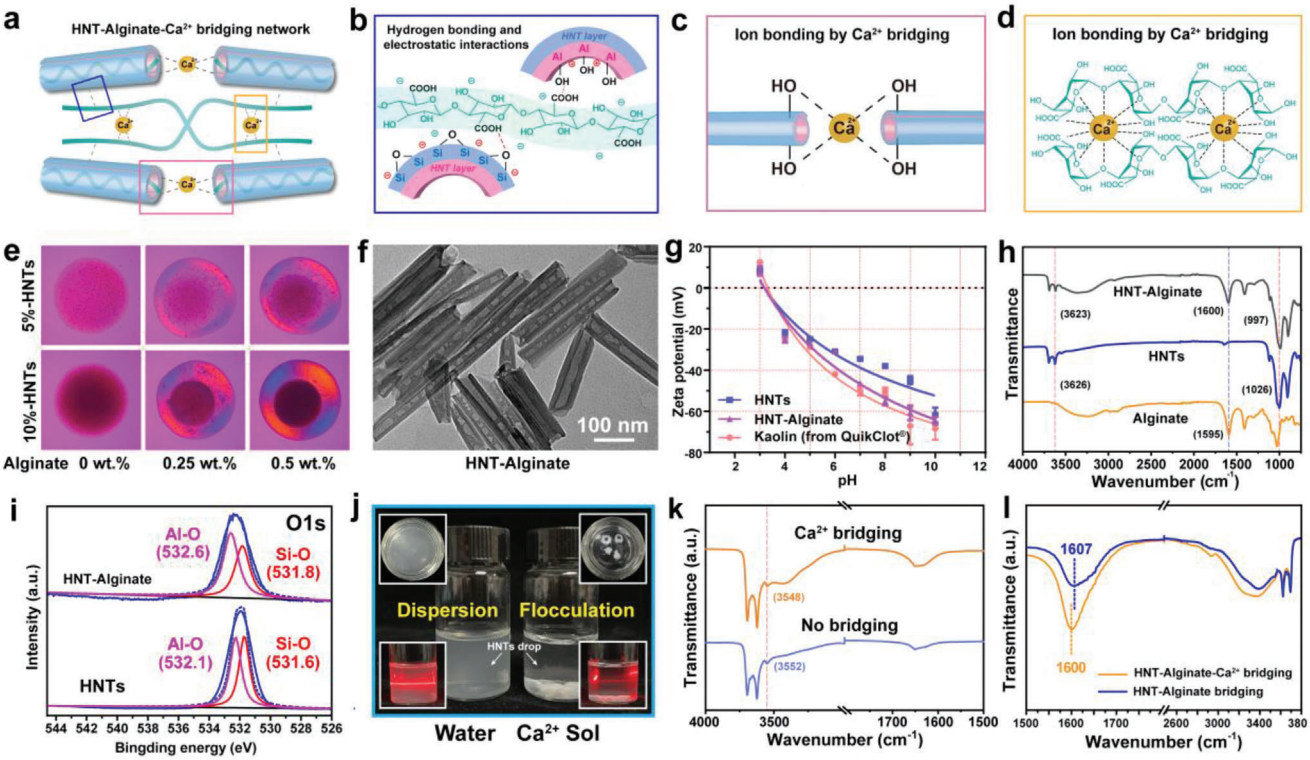


**Figure 1.** HNT-alginate-$Ca^{2+}$ network bridged by electrostatic adsorption and hydrogen and ionic bonding. Schematics for a) HNT-alginate-$Ca^{2+}$ bridging network, b) HNTs hydrogen bonding by alginate bridging, c) ionic bonding by $Ca^{2+}$ bridging, and d) alginate crosslinking with $Ca^{2+}$ and "egg box" structures. e) The polarized optical images of alginate mediate the display of liquid crystals in the coffee ring of HNTs. f) TEM images of HNT-alginate. g) The $\zeta$-potential of HNTs, HNT-alginate, and kaolin (originated from QuikClot) ranges from pH = 3 to pH = 10. h) FTIR spectra of HNTs with no bridging, alginate and alginate bridged HNTs, confirming the hydrogen bonding. i) O1s XPS spectra of HNTs with or without alginate bridging. j) HNTs droplets flocculate in $Ca^{2+}$ solution, demonstrating the presence of ionic bonding. k,l) The localized magnified FTIR spectra of HNTs or HNT-alginate with or without $Ca^{2+}$ bridging.

peaks of O1s, Si 2p/2s, and Al 2p/2s, which are attributable to the characteristic elements of HNTs (O, Si, and Al). The strong C1s peak in the HNT-alginate spectrum indicates the successful combination of alginate and HNTs. Furthermore, the transmission electron microscope (TEM) images show that the polymers are mainly distributed in the inner lumen of HNTs (Figure 1f). HNTs exhibit positively charged inner lumen, which consist mostly of aluminum hydroxide, and a negatively charged outer surface, which consists of silicon dioxide.[35] Alginate is negatively charged due to the carboxyl groups on the molecular chains. Therefore, the negatively charged alginate enters the inner lumen of HNTs more than on the outer surfaces due to the electrostatic attractions. As shown in Figure 1g, the entry of alginate neutralizes the positive charge and increases the total negative charge of HNTs. With increasing alginate content from 0 to 9 mg $mL^{-1}$, the $\zeta$-potential of HNT-alginate changes from $-36.8 \pm 0.4$ to $-37.6 \pm 3.2$ mV, $-59.2 \pm 1.7$ mV, and $-73.6 \pm 3.2$ mV, respectively (Figure S5, Supporting Information). Deposition of negatively charged compounds inside the inner lumen of HNTs will neutralize internal positive charges and drastically increase the overall nanotube negativity, changing the $\xi$-potential to $\approx -70$ mV.[36] These results indicate electrostatic interactions between HNTs and alginate. Kaolin used in QuikClot combat gauze dressings has a high negative charge than raw kaolin, possibly due to the addition of anionic dispersants such as hexametaphosphate (to improve dispersibility).[37]

Except for electrostatic attraction, FTIR spectra (Figure 1h) further confirms the molecular-level interactions between HNTs and alginate. The C = O stretching vibration of alginate and the Al–OH stretching vibration of HNTs are shifted from 1595 and 3626 to 1652 and 3623 $cm^{-1}$, respectively. The Si–O–Si stretching vibration is also shifted from 1026 to 997 $cm^{-1}$. This is probably owing to the hydrogen bonding (O–H ... O) at the HNTs/alginate interfaces. XPS results (Figure 1i) show that the O1s fitted peaks of HNTs associated with Al–O and Si–O lattice oxygen shift from lower binding energies (532.1 and 531.6 eV) to higher binding energies (532.6 and 531.8 eV) in HNT-alginate sample, respectively. This change also indicates that the interactions between alginate with HNTs change the chemical environment at the Si–O and Al–O interfaces. In addition, flocculation is observed after dropping HNT droplets into a $Ca^{2+}$ solution instead of forming dispersed colloids with a Tyndall effect in water (Figure 1j). Besides, the shift of the –OH peak of HNTs to 3548 $cm^{-1}$ is also observed in $Ca^{2+}$-bridged HNTs, indicating the formation of H–O→$Ca^{2+}$ coordination between $Ca^{2+}$ and HNTs (Figure 1k). The presence of $Ca^{2+}$ also shifts the C = O stretching peak of the alginate in HNT-alginate from 1607 to 1600 $cm^{-1}$, which verifies the coordination between HNT-alginate and $Ca^{2+}$ (Figure 1l). In summary,

 

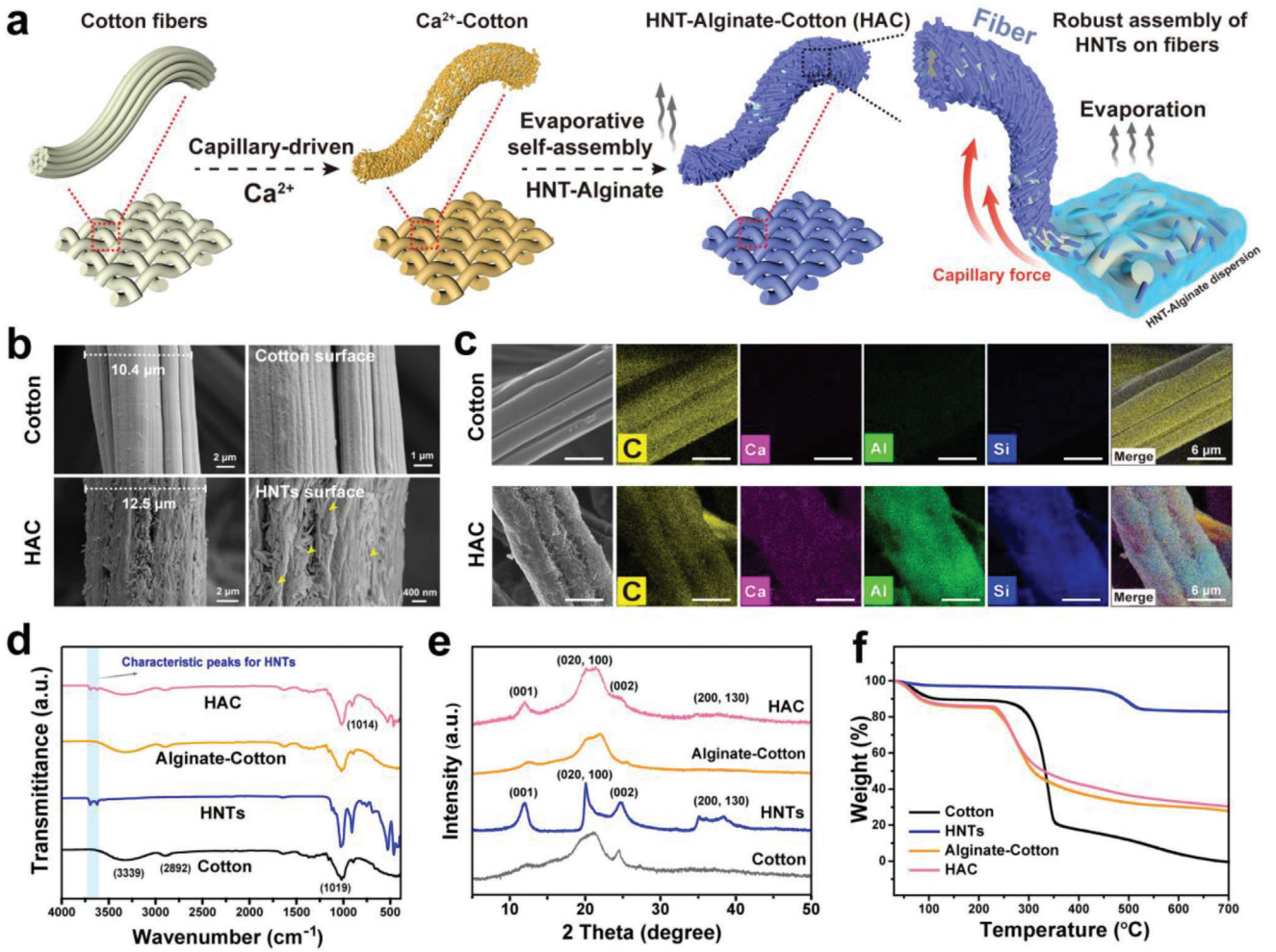


**Figure 2.** Preparation and characterization of HAC. a) Schematic showing fabrication of robust assembly of HNTs on fibers. b) SEM images of HNTs on a single fiber (the thickness of the coating is about 2 μm). c) EDS mapping analysis images for cotton and HAC, Al (green) and Si (blue) indicate the HNTs layer. d) FTIR spectra, e) XRD patterns, and f) TGA of cotton, HNTs, Alginate-Cotton, and HAC.

hydrogen bindings and electrostatic attraction between alginate and HNTs trigger the assembly of the nanotubes, and ionic bonding with $Ca^{2+}$ stabilizes the assembled structure. These bonds play an essential role in the robust self-assembly of HNTs on fibers, which will be demonstrated below.

### 2.2. Robust Assembly of HNTs on Cotton Fibers Mediated by Capillary Effect and Ion Diffusion

The robust assembly of HNTs on cotton fibers driven by the capillary effect and mediated by $Ca^{2+}$ ions is schematically shown in **Figure 2**a. Cotton dressings have a long history as hemostatic fabrics, and cotton fibers are commonly used for dressing materials due to their superior surface wettability, porous structure, and capillary action between the woven fibers.[3] The preparation includes two parts: the enrichment of $Ca^{2+}$ on cotton fibers and the compounding of HNT-alginate. To create a $Ca^{2+}$ rich interfaces of fiber, the commercial cotton fabric was immersed in a $Ca^{2+}$ solution (20 mM) until saturation and then dried to obtain $Ca^{2+}$-Cotton. The swelling-contraction process (accompanied by wetting and evaporation) of hydrophilic porous fibers allows the ions to penetrate thoroughly into the fiber structure. Simultaneously, solutions with different alginate-HNT mass ratios (shown in Figure S6, Supporting Information, with 0.6:1 as the optimal) were stirred overnight. The $Ca^{2+}$-Cotton was vertically placed in HNT-alginate dispersion and dried to obtain HAC. During this process, HNT-alginate liquid moves along the fibers due to the capillary force of the hydrophilic fabric, and the high ionic concentration at the interfaces also tows HNT-alginate enrichment on the fiber surface due to ionic bonds with alginate and HNTs.

Subsequently, evaporation provides kinetic support for nanotube assembly and further forms a robust nanotube-biopolymer network on the fibers. In the evaporation process, the liquid evaporation rate at the liquid's three-phase (solid–liquid–gas) contact interface is significantly stronger than at the liquid–gas interface. Therefore, a convective flow causes continuously replenishes the outer edge, forming a continuous quantitative assembly of nanotubes to the fiber surface (Figure 2a, right). According to Figure 1, alginates tend to enter the lumen of HNTs by electrostatic

 

gravity because of the negatively charged carboxyl groups on their molecular chains. Moreover, their carboxyl groups can form hydrogen bonds with the hydroxyl groups of HNTs, including Al–OH in the lumen and a few Si–OH located in HNT ends and surface defects.[38] The addition of alginate improves the water dispersibility and stability of HNTs dispersion, which are essential for their uniform assembly. It can also increase the dispersion viscosity and retard the free movement of HNTs, contributing to the homogeneous and ordered alignment of the tubes. More importantly, $Ca^{2+}$ ions in the fiber form a stable three-dimensional HNT-alginate network through ionic cross-linking. By evaporation, a strong "chain" structure through the fiber was formed, anchoring the HNTs tightly on the fiber.[26] Washing experiments (Figure S6, Supporting Information) demonstrate that HAC prepared at alginate: HNTs mass ratio of 0.6:1 is best for capillary and ion-driven assembly to produce non-shedding HNTs coatings for following safe and rapid hemostasis application.

This method utilizes the electrostatic attraction of opposite charges between different layers to enrich nanotubes to the fiber substrate while introducing hydrogen bonding and ionic cross-linking to improve the robustness.[39] Assembly of raw HNTs on natural and synthetic fibers without using interfacial adhesive was explored in previous studies.[13,21] In those cases, HNTs coatings were not stable at the fiber surfaces which were easily peeled off from the matrix. If using only alginate alone without $Ca^{2+}$, HNT-alginate cannot form a robust polymer network on the fibers, resulting in dissolution and detachment of the coating in aqueous systems.

Scanning electron microscope (SEM) images (Figure 2b and Figure S7, Supporting Information) display that the HAC retain the original morphological features of the fabric compared to the uncoated cotton, and the HNT-alginate coating cover the overall surfaces of each fiber with a thickness of ≈2 μm. Some of the nanotubes are arranged in parallel along the fiber axes, but the assembly does not show significant regularity due to the unevenness of the fiber surface and the non-ideal single-fiber evaporation process. Energy dispersive spectroscopy (EDS) mapping analysis (Figure 2c and Figure S8, Supporting Information) shows the distribution of Ca, Al, and Si elements (indicative of HNTs) in HAC fibers with normalized mass percentages of 8.1%, 14.0%, and 16.5%, respectively. This assembly strategy can be successfully applied to hydrophilic fibers (e.g., cotton gauze, cotton nonwovens, elastic bandages, and blended cotton fabrics) (Figure S9, Supporting Information). Some hydrophobic fibers, which are poor $Ca^{2+}$ reservoirs due to their smooth surface, also see non-uniform adhesion of HNTs on the fiber surface (Figure S10, Supporting Information).

FTIR spectroscopy (Figure 2d and Figure S1g, Supporting Information) was used to further characterize the successful coating of HNTs on HAC. The characteristic peaks for HNTs appear in the HAC sample (Figure 2d, green zone). The broad peak at ≈3339 $cm^{-1}$ in cotton fiber can be attributed to the –OH group of cellulose and water, and 2892 and 1019 $cm^{-1}$ can be assigned to C–H stretching vibration and C–O stretching, respectively.[40] C–O stretching vibration peaks around 1019 $cm^{-1}$ of cellulose are shifted to 1014 $cm^{-1}$ in the HAC sample, probably due to hydrogen bonding at the HNT–alginate–cellulose interface.

The assembly of HNTs on HAC can also be confirmed by X-ray diffraction (XRD) patterns in Figure 2e and Figure S1h (Supporting Information). The characteristic peaks of HNTs are observed at 11.9° (001), 20.1° (020, 110), 24.7° (002), 35.0–40.0° (003, 130) (ICDD No. 29-1487).[41] The diffraction peak at 11.51° (001) corresponds to a layer spacing of 7.41 Å.[42] Cotton fibers and alginate are semi-crystalline and show no distinct peaks in the pattern except for the cellulose peak (24.46°). Compared to alginate-coated cotton (Alginate-Cotton), HAC shows several diffraction peaks attributed to HNTs, indicating high HNTs content on the surfaces of HAC. Thermogravimetric analysis (TGA) reveals that the ternary component (HNT-alginate-$Ca^{2+}$) loading on the HAC dressing is ≈34.2% (Figure 2f). It is noticed that the TGA curves of Alginate-Cotton and HAC are close due to the lower mass fraction of HNTs. Benefiting from the superior procoagulant activity of HNTs, a small amount of HNTs can achieve satisfactory hemostasis.[43] The thermogravimetric differential curve (DTG) curves (Figure S11, Supporting Information) show that the degradation peak of Alginate-Cotton is at 266 °C, while HAC has a slightly higher degradation temperature at 274 °C, which is probably due to the heat-resistant of clay layers in HNT-alginate.

### 2.3. Flexibility, Wettability, Absorbability, and Breathability of HAC

The robust assembly of HNTs on the HAC does not affect cotton fibers' flexibility (easily twisted 360° in situ) (**Figure 3**a), allowing for great potential for hemostasis on different tissue surfaces. As shown in Figure 3b, the dispersed HNTs on the dressing improve the blood wettability of the fibers (contact angle from 70.9 ± 8.8° for cotton to 40.0 ± 2.8° for HNT-Cotton and 37.9 ± 2.6° for HAC, slightly less than 43.9 ± 2.8° for QuikClot combat gauze). The water contact angle results are mainly affected by surface roughness, and the apparent contact angle decreases for hydrophilic materials.[44] As shown in Figure S12 (Supporting Information), the hydrophilic nanotubes assembled on the surface of HAC increase the roughness and thus reduce the contact angle. In addition, the capillary action of the nanotubes rapidly absorbs water, resulting in a smaller contact angle, and blood factors are concentrated on the fiber surface, thereby improving the hemostatic properties.[13,45] Absorbability to water and blood is not significant difference in the raw cotton group. However, HNT-loaded dressings show enhanced blood adsorption ability compared with the water, which is probably explained the local attachment by the blood cells to the treated fiber surface by the capillary force of the nanotubes. This phenomenon arises from the blood concentration-aggregation effect of HNTs, implying a stronger clotting activity of HAC (Figure 3c).

The liquid absorption rate was then evaluated by hanging up these dressings on the diluted blood sample surfaces, and there was no significant difference between all groups, whether treatment or not (Figure 3d). Interestingly, the HAC group shows a molecular sieve effect on the blood components in the liquid, and no erythrocytes can climb up to the top of the dressing, which is not observed in the HNT-Cotton and Alginate-Cotton groups. This phenomenon implies that capillary-ion-mediated HNTs assembly may have micro-nano scale orderliness. The hydrophilic clay nanotubes arranged on the fibers, which only allows water molecules but blocks the penetration of erythrocytes. This effect causes the concentration of blood on the dressing to accelerate blood clotting.[46] The water vapor transmission test

 

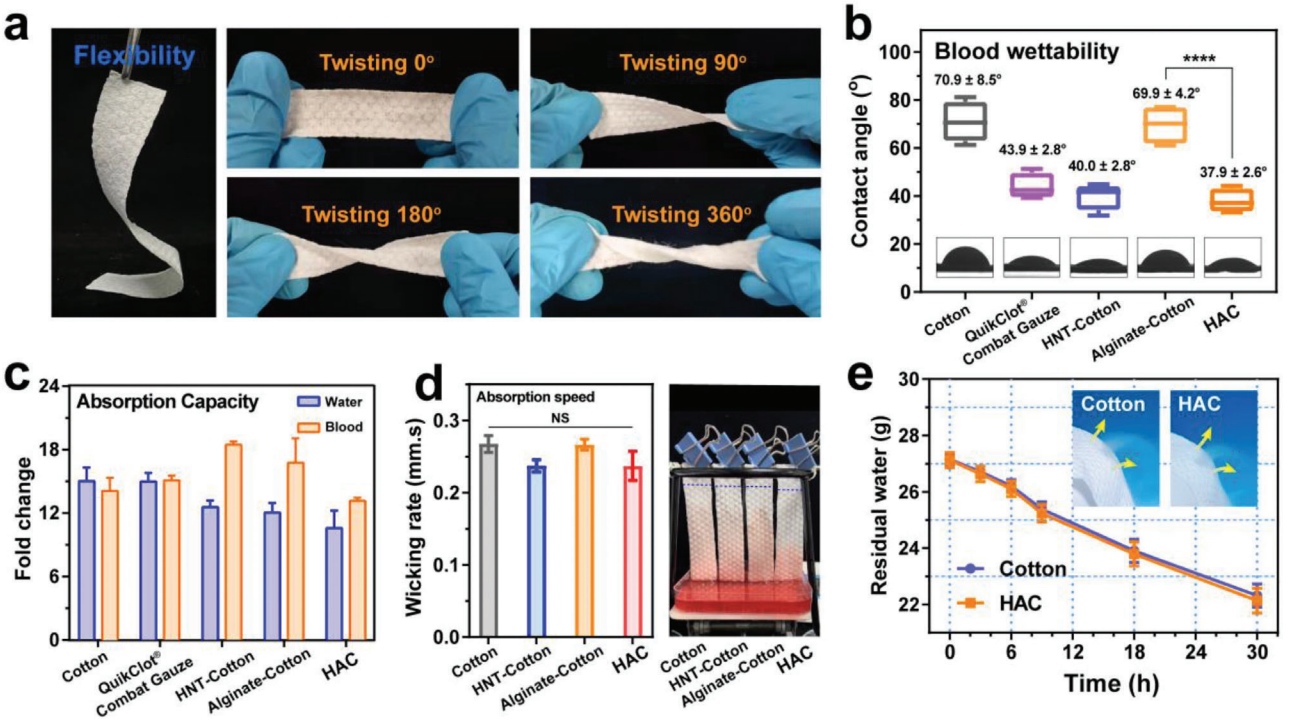


**Figure 3.** Evaluation of flexibility, wettability, absorbability and permeability of dressings. a) Photographs of fabrics with varying degrees of in situ twisting demonstrate their flexibility. b) Blood contact angles and c) water or blood absorption capacity for cotton, QuikClot combat gauze, HNT-Cotton, Alginate-Cotton, and HAC. d) Aspiration speed of cotton, HNT-Cotton, Alginate-Cotton, and HAC. The dry–wet boundary is marked with blue dashed lines. e) Water vapor transmission test of cotton and HAC. Data were expressed as mean ± standard deviation (SD), ****$p < 0.0001$, NS means no significant.

(Figure 3e) display that HAC maintains the good permeability of cotton, demonstrating that the three-dimensional structure formed by HNT-alginate on cotton fibers does not significantly affect the porosity of the dressing. This is beneficial to the oxygen exchange in the wound area, which is a critical factor in promoting wound closure.[47] Nitrogen adsorption isotherms (Figure S13, Supporting Information) illustrate the enhanced adsorption capacity of fiber surface after HNT-alginate assembly. The large porosity of HNTs increases the surface area of cotton, which will be beneficial to hemostatic activity.[4]

### 2.4. Robustness and In Vitro Hemostatic Performance Evaluation

Cotton-based hemostatic dressings are the most used in clinical treatment, which possess the advantages of convenience, flexibility, and portability. For example, kaolin-impregnated dressing QuikClot combat gauze is the most widely used in hospitals and the military. Unfortunately, kaolin has a weak binding state with the dressing fibers (Figure S14, Supporting Information). The peel-offed kaolin may penetrate the wound and cause inflammation, distal thrombosis, and even the risk of amputation.[5a]

Indeed, as shown in **Figure 4**a, severe exfoliation of kaolin powder is observed immediately after dipping QuikClot combat gauze into the water. Likewise, HNT-coated cotton fibers prepared by impregnation (cotton fabric soaked in HNTs suspension, then dried and labeled as HNT-Cotton) are not immune. In contrast, HNTs assembled on the dressing by alginate have superior robustness with almost no powder entering in water. In addition, the stability of the hemostatic dressing in the face of fluid flushing is critical, as the influx of large amounts of blood may lead to failure of the unsound hemostatic component in practice.[4] Subsequently, we repeatedly flushed the material with deionized water under ultrasonication treatment to simulate the peel-off situation during the hemostats process. The shedding amount of coagulation components on the dressing after washing is shown in Figure 4b. After 2 min of treatment, QuikClot and HNT-Cotton lose 95% and 92% of clay, respectively, while more than 80% of coagulation components in HAC dressing are retained. The increased binding between HNTs and cotton fibers is attributed to the interfacial interactions between the alginate and $Ca^{2+}$ in this system. Since identifying powder peel-off from the fibers by the native eye is difficult, we subsequently monitored the wounds treated by fluorescein isothiocyanate (FITC)-labeled QuikClot combat gauze and FITC labeled HNTs prepared HAC using in vivo fluorescence imaging (Figure 4c and Figure S15, Supporting Information). ≈60.5% of the kaolin was peeled off (based on total fluorescence area) in the QuikClot combat gauze group from the heavy staining of the wounds, while fluorescent HNTs barely stained the wounds. Since foreign matter with coagulable activity could bring health risks,[5b] this work aimed at providing a promising strategy for developing robust hemostatic agents.

Apart from preventing the health risks arising from shedding, a robust hemostatic dressing also minimizes the loss of hemostatic components to retain maximum clotting activity. The clotting test (Figure 4d) reveals that HNTs addition considerably reduces whole blood clotting time from 301 ± 17 s (Cotton) to

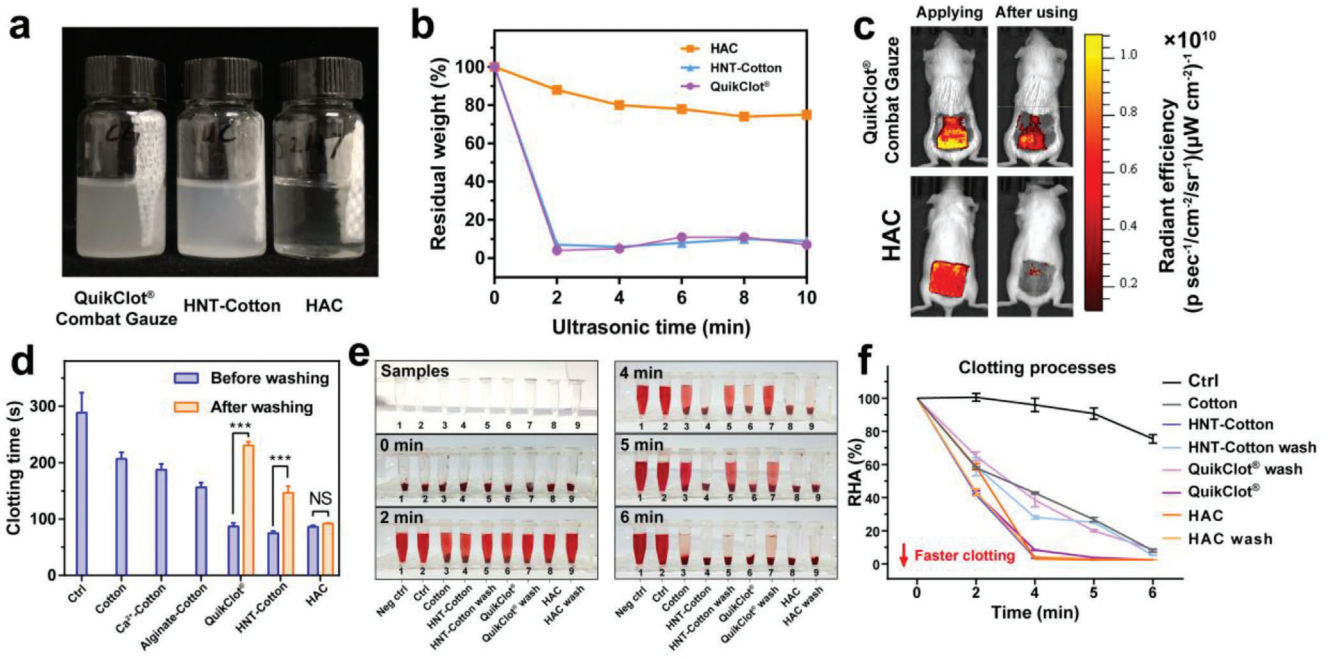


**Figure 4.** Robustness of the hemostatic component and the clotting ability maintained after washing. a) Photographs of QuikClot combat gauze, HNT-Cotton and HAC after immersing into the water and sonicating for 10 min. b) The relative residual weight of hemostatic component on QuikClot combat gauze, HNT-Cotton and HAC after different ultrasonic times. c) In vivo fluorescence imaging photos of mice skin wounds during and after being treated with FITC-labeled QuikClot combat gauze and HAC. d) The whole blood clotting time of fabrics before and after washing. e) Photographs of the in vitro blood-clotting tests, and f) the relative hemoglobin percentage reflects the clotting process of each sample at time points. Bars were represented as mean ± SD ($n = 4$). Unpaired Student's *t*-test, two-tailed, $^{***}p < 0.001$, NS means no significant.

80 ± 3 s (HNT-Cotton) and that the procoagulant activity of HAC is virtually unaffected after washing. The clotting activity of the HAC materials is mainly dependent on the outer surface properties of HNTs, including negatively charged surfaced and glass effect to activate clotting factors.[48] In contrast, the extensive loss of hemostatic components of QuikClot combat gauze or HNT-Cotton after water washing resulted in delayed coagulation. Clotting is the process by which blood changes from a liquid to a gel, forming a blood clot, and erythrocytes are gradually trapped by fibrin along with the process. Thus, the clotting process can be monitored by the release of erythrocytes (in the form of free hemoglobin) from the clot in water (Figure 4e), and a lower percentage of relative hemoglobin (normalized to the uncoagulated state) means more mature clots and faster clotting rates (Figure 4f). Consistent with the trend in Figure 4d, wash treatment severely retards HNT-Cotton and QuikClot coagulation (blue and purple lines). On the contrary, the robustness of HAC (orange line) maintains its superior procoagulant activity after washing (Figure 4e,f). It should be noticed that $Ca^{2+}$ ions and alginate also contributed to the enhanced procoagulant effect (Figure S16, Supporting Information). Alginate can assist in clot formation by altering the rheological properties of the blood (Figure S16c, Supporting Information).

### 2.5. Material–Blood Interactions

The coagulation mechanisms of HAC are further analyzed by flow cytometry (FCM), solid surface zeta potential, SEM images, and thromboelastography (TEG). In a representative FCM analysis result (**Figure 5**a), the percentage of $CD61^+/CD62P^+$ cells increase incrementally (from 4.8% to 10.3%) with increasing HAC dressing dosage. The statistical diagram of FCM results (Figure 5b) shows that the percentage of $CD61^+/CD62P^+$ cells in the HAC group (10.2 ± 1.2%) compared to the blank group (positive control) of 14.4 ± 2.0%, which is higher than that of 5.6 ± 0.9% in the blank group, indicating that HAC had a good effect on platelet activation.[13]

Negatively charged surfaces are known to contribute to the activation of coagulation factor XII to initiate the intrinsic clotting pathway, so the surface potential of the dressing has an essential effect on coagulation.[49] According to Figure 1g and Figure S5 (Supporting Information), the bridging of alginate with HNTs significantly improved surface negative charge. The solid surface potential results (Figure 5c) also reveal that the alginate modification increased the negative charge of the dressing slightly (−23.4 ± 1.8 mV) compared to the original cotton dressing (13.1 ± 0.8 mV). In comparison, adding clay to the HAC increased the negative charge considerably (−31.2 ± 1.6 mV), comparable to QuikClot combat gauze (−29.4 ± 1.0 mV). Moreover, a large number of erythrocytes aggregate on the HAC dressing (Figure 5d and Figure S17, Supporting Information, suggesting that polymeric network structure formed by HNT-alginate-$Ca^{2+}$ helps to restrict blood flow and trap blood cells.[9] Individual fiber surface microplots formation, including platelet activation, was observed by SEM (Figure 5d). Fibrinogen forms fibrin to trap blood cells further. This process is primarily mediated by the coating of HNTs on the surface of HAC fibers.

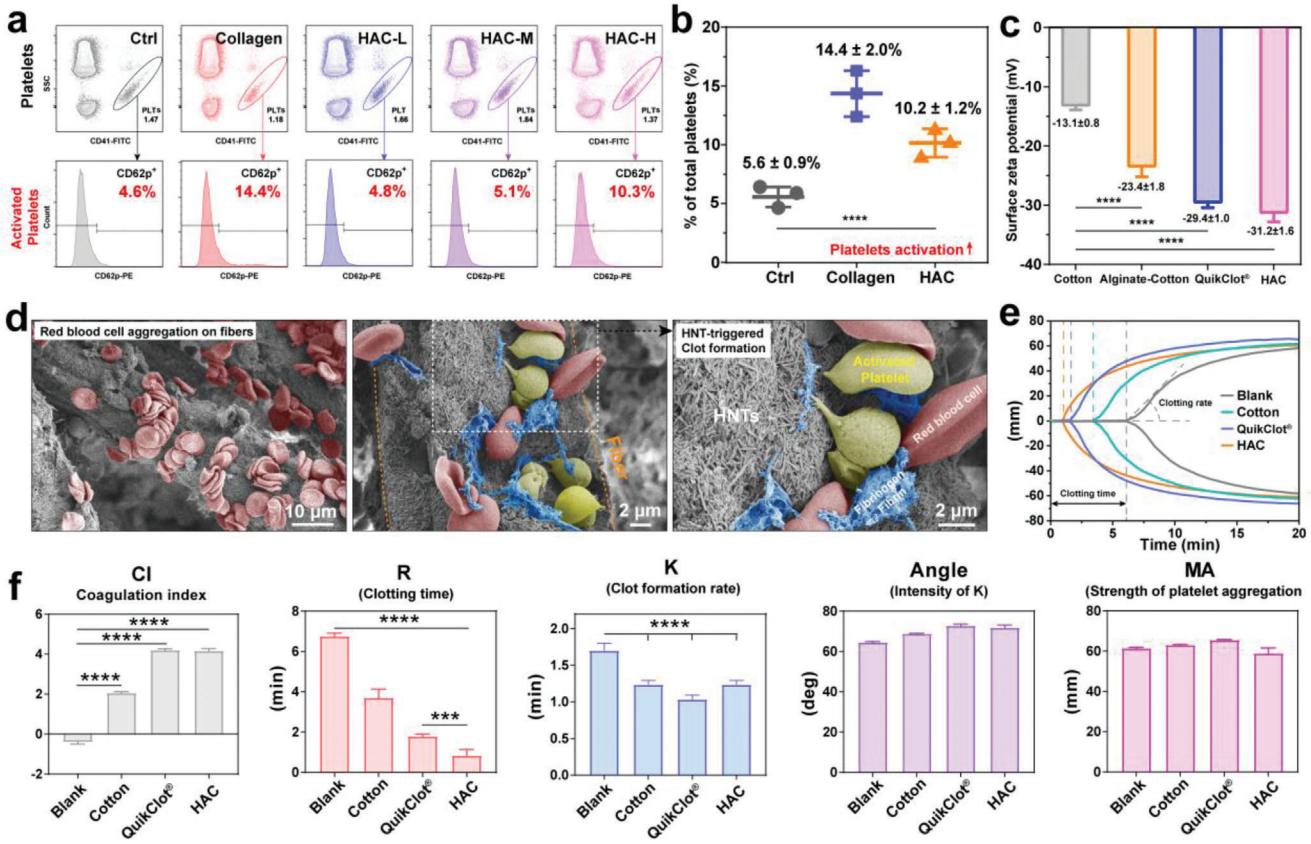


**Figure 5.** Coagulation mechanisms and blood cell–robust coating interface interactions. a) The representative FCM graphs show the percentage of $CD61^+/CD62P^+$ cells (activated platelets) after being treated with collagen (positive control) or HAC from low to high dose. Raw blood as for blank control. b) Statistics for FCM analysis of blank control, collagen, and HAC (high doses), displaying the activation rate of platelets. c) Surface zeta potential of cotton, Alginate-Cotton, QuikClot combat gauze and HAC. d) The SEM images of blood components' interaction with the HAC fibers and HNTs coating. Red represents erythrocytes, yellow represents platelets, and blue represents fibrins, respectively. e) The traces and f) values of TEG of the whole blood samples after function with cotton, QuikClot combat gauze, HAC and without materials (blank group), $n = 3$. (CI: Coagulation composite index, R: Reaction time, MA: Maximum amplitude, K: Clot formation time, Angle: $\alpha^\circ$ of the greatest amplitude on the TEG trace.) Data are expressed as mean ± SD; $^{****}p < 0.0001$. Student's *t*-test (two-sided) was used for statistical analysis of between two groups comparison.

In TEG analysis (Figure 5e and Figure S18, Supporting Information), the HAC group (coagulation composite index CI: 3.9; reaction time R: 0.9 min) is significantly outperforming the blank group (CI: 0.4; R: 6.5 min), while the value of the QuikClot combat gauze group is CI: 4.1 and R: 1.6 min. Furthermore, the clot formation time (*R*-value) is shortened, and the angle is increased, reflecting the more rapid clot formation by HAC. The maximum amplitude (MA) is in the normal range in the HAC group, indicating a function of clot strength maintenance at an average level. In a word, HNTs coating on HACs can activate platelets, accelerate the aggregation of blood components, and trigger the contact coagulation process (intrinsic coagulation pathway, including clotting factor activation, fibrin generation, and formation of the final clot). TEG analysis of several clays (including laponite, kaolin, HNTs, and attapulgite) show that the kaolin and HNTs have superior advantage in coagulation, and the rod-like attapulgite also perform well, but laponite shows insufficient activity (Figure S19, Supporting Information). Previous studies suggested that exposure of whole blood to the kaolin family activated kininogen, plasma kinin-releasing enzyme and XII factors to trigger the clotting process.[49] HNTs are formed by kaolin rolling, so their procoagulant activity is related to the inorganic–biological contact interface of silicate.[50]

### 2.6. HAC Mediates Rapid and Effective Hemostasis in Organs and Vascular Bleeding Models

Different hemostatic materials of similar mass (≈500 mg) for visceral hemostatic performance are evaluated using a rat liver bleeding model (**Figure 6**a). It is observed that the addition of kaolin (QuikClot combat gauze, see Movie S1, Supporting Information) and HNTs (HNT-Cotton, HAC, see Movies S2 and S3, Supporting Information, respectively) accelerate the hemostatic process and allowed complete wound coagulation within 3–4 min. But the cotton dressings are still bleeding until 5–6 min (Figure 6b and Movie S4, Supporting Information). The superior procoagulant ability of HNTs excites its fluidic state to a solid state once it contacts blood (Figure S20, Supporting Information), resulting in a reduction of blood infiltration in multilayer dressings (Figure 6c). Wounds treated with cotton lose 3.06 ± 0.90 g of blood, and commercial QuikClot combat gauze dressings and

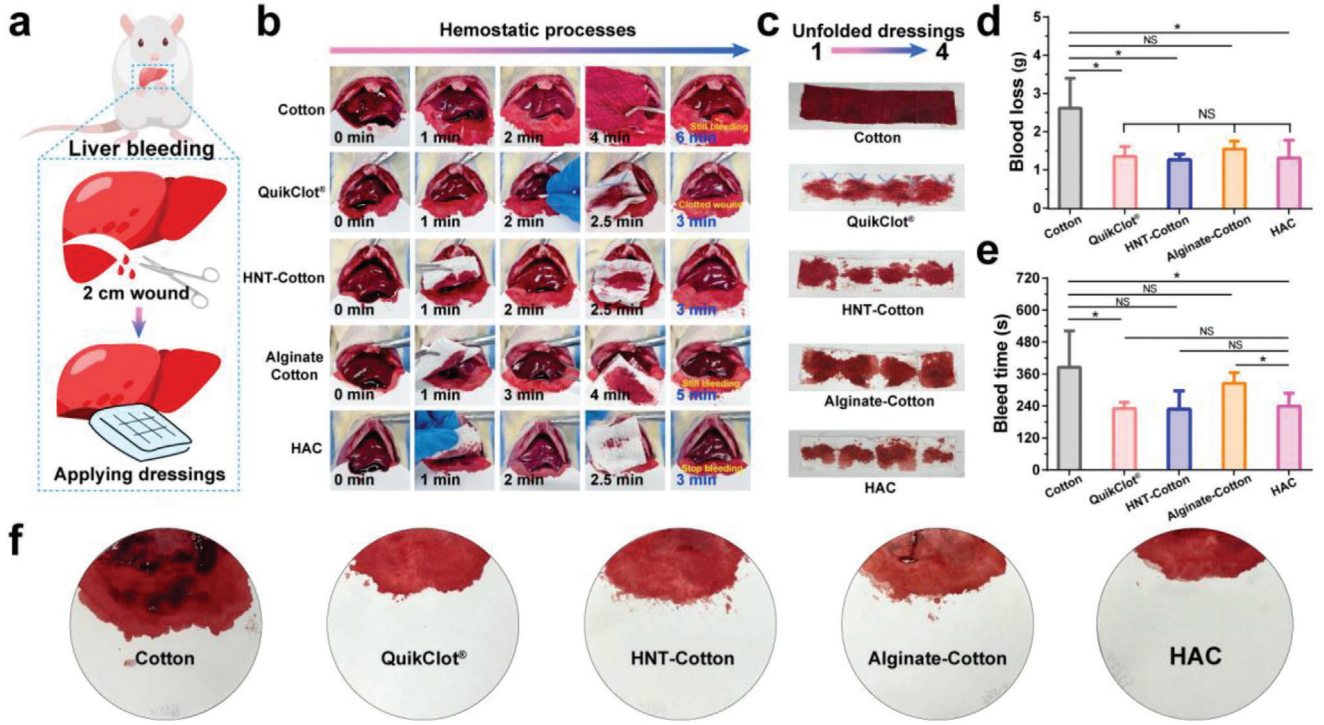


**Figure 6.** Instant hemostatic evaluation of rat liver. a) Schematic diagram of induced hemorrhage in rat liver and hemostasis with different hemostatic dressings. b) Photographs of bleeding and hemostatic processes after applying different dressings, and the last photo shows the final time to stop bleeding. c) Photos of the dressing removed from the wound after hemostasis, with four layers of the stacked dressing unfolding. d) Blood loss and e) bleeding time in this model. f) Representative photographs of blood remaining on filter paper indicate total blood loss. Statistical significance is considered as $*p < 0.05$, NS means no significant. Data are shown as the mean ± SD, and differences in the means of the group were analyzed by one-way analysis of variance (ANOVA), $n = 5$.

HNT-Cotton dressings reduce blood loss to 1.40 ± 0.25 g and 1.20 ± 0.15 g, respectively. HAC retains the strong procoagulant function of HNTs (1.31 ± 0.46 g), which is not significantly different from QuikClot combat gauze and HNT-Cotton. These results reveal that the HNT-modified dressings all show strong hemostatic promotion superior to common cotton fibers. Alginate-coated fibers (1.71 ± 0.37 g) show slightly weaker hemostasis ability relative to clay groups (Figure 6d–f). In Figure 6e, the shortening of hemostasis time relative to cotton (385 ± 137 s) is evident in the clay groups (QuikClot combat gauze: 235 ± 20 s; HNT-Cotton: 228 ± 69 s; HAC: 240 ± 49 s), while alginate (322 ± 33 s) is unable to accelerate coagulation significantly (Movie S5, Supporting Information). These results are consistent with previous studies, and modification of natural biopolymers with HNTs significantly improved procoagulant activity.[51]

The rat femoral artery injury model (**Figure 7**a) is used to evaluate the hemostatic effect of gauze on heavy bleeding. Analogous to the rat liver injury model, both kaolin-based QuikClot combat gauze and HNT-based HNT-Cotton and HAC perform outstandingly. As shown in Figure 7b, each clay-containing dressing can fully clot the wound in around 3 min, but the cotton group is still bleeding (Movie S6, Supporting Information), and the Alginate-Cotton group is still oozing blood (Movie S7, Supporting Information). The blood loss of cotton, QuikClot combat gauze, HNT-Cotton, Alginate-Cotton, and HAC dressings are 7.29 ± 1.48, 3.51 ± 1.45, 3.14 ± 1.64, 6.22 ± 1.79, and 2.95 ± 1.55 g, respectively (Figure 7c). In addition, the hemostasis times of cotton, commercial QuikClot combat gauze (Movie S8, Supporting Information), HNT-Cotton (Movie S9, Supporting Information), Alginate-Cotton, and HAC dressings (Movie S10, Supporting Information) are 349 ± 131, 211 ± 89, 157 ± 23, 349 ± 82, and 150 ± 23 s, respectively (Figure 7d). There is a noticeable reduction in blood maceration on the dressings, and the amount of dressing required to stop bleeding is reduced from 3 to 1 piece (Figure 7e). Compared with cotton dressing, HAC dressing respectively reduces hemostasis time and blood loss by 57% and 59%. In this model, the hemostatic effect of HAC is slightly better than that of QuikClot combat gauze, which may be due to the loose kaolin on QuikClot combat gauze being wash away by the massive blood flow, causing a deterioration in performance. No matter in the liver or femoral arterial-venous bleeding model, most animals survive after HAC dressing application (Figure S21, Supporting Information). In summary, the high hemostatic capacity of HAC for the vascular injury hemorrhage model is as effective as for the liver injury model.

In conclusion, the strongly procoagulant HNTs coated dressings (regardless of whether tightly and loosely bound) show excellent control of bleeding due to their blood concentration and strong activation of platelets and coagulation pathways.[13] The alginate-based method of robust assembly of HNTs makes the wound dressing less susceptible to fail and retains complete functionality, which is an essential benefit for post-hemostasis wound care and systemic safety. The following work of the prepared high-performance HAC dressing can be extended to loading

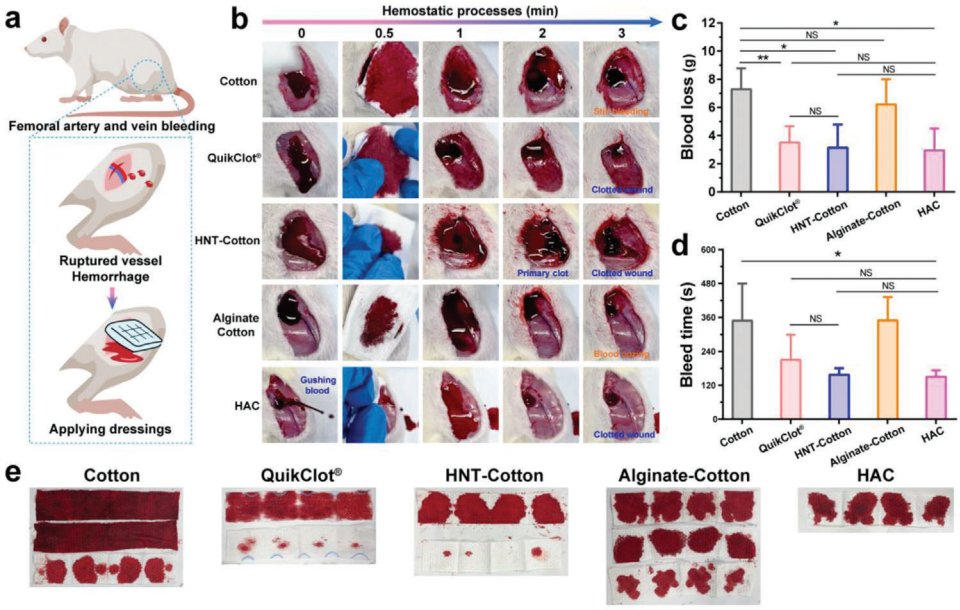


**Figure 7.** Hemostatic performance of dressings on the rat femoral arterial-venous injury. a) Schematic illustration of surgery and hemostasis procedure. b) Photographs of the bleeding and hemostasis process within 3 min. c) Blood loss, and d) bleeding time in this model. e) Photos of the dressings used to stop bleeding, the number of dressings and stained blood suggests the total amount of bleeding. Data are shown as the mean ± SD, and ANOVA is used to analyze the differences in the means of the groups, $*p < 0.05$ and $**p < 0.01$, NS means no significan, $n = 5$.

antibacterial agents or drugs to HNTs. For instance, infection is also a severe health risk after traumatic bleeding. Encapsulation of antibiotics, particularly within nanoscale containers, has the potential for prolonged release, and HNT lumen is especially suitable for drug encapsulation.[52] Encapsulating antibiotics in HNTs in future work can synergize hemostasis and anti-infection, thereby meeting the needs of trauma prehospital care.

### 2.7. Biocompatibility of Materials

The biosafety of hemostatic dressings is of practical importance for application. The high biocompatibility of HNTs and alginate are already known in medical applications, and the robust assembly further prevents the safety risk of hemostatic material detachment.[26,53] Cellular experiments prove that the HAC has good cytocompatibility (**Figure 8**a–c). The cell viability by Cell Counting Kit 8 (CCK-8) method, live–dead staining, and apoptosis results of the material leachates show above 90% cell viability, which is in the cytotoxicity grading of 0–1, proving that the material is non-cytotoxic.[54] The alginate-mediated assembly also promotes the hemocompatibility of the dressings. The hemolysis rates of Alginate-Cotton and HAC are as low as 1.6% and 1.7%, respectively, in contrast to 7.6% and 9.3% for QuikClot combat gauze and HNT-Cotton (Figure 8d). The reduced erythrocyte breakage can be explained by a decrease of shedding clay. To further confirm the biosafety of the materials, HAC was embedded in the subcutaneous tissue of the rat back (Figure 8e). After 7 days, alginate-mediated HNTs assembly (Alginate-Cotton and HAC) enable a thinner fibrous envelope to the dressing (Figure 8f and Figure S22, Supporting Information), indicating good biosafety of HAC.

## 3. Conclusion

In conclusion, alginate is used to bridge halloysite clay nanotubes in the presence of ion diffusion-capillary effect, which provides a strategy to achieve robust anchoring of these nanoclays on fibers. The clays coated fibers show favorable changes in surface morphology, adsorption, water absorption, blood clotting property, and hemolysis ratio. Alginate interacts with HNTs through hydrogen bonding and electrostatic attraction, which promote dispersion and surface assembly of the tubes in an aqueous system. HNT-alginate forms a robust coating of the fiber via $Ca^{2+}$ ionic bonding, which firmly anchors the high-performance hemostatic agents on the hydrophilic fibers. Clay nanotubes are uniformly arranged with a thickness of 2–3 μm on the surfaces of cotton fibers with a low loss after washing, and the residual in the wounds is minimal. Therefore, this composite dressing maintains high hemostatic activity even after washing assuming high formulation stability in a wet state. The hepatic and vascular hemorrhage model show that the prepared dressing has more comprehensive performance and higher biosafety than the commercial QuikClot combat gauze. This work provides a reliable method to assemble nanoclays on fibers, which results in an efficient, robust, low tissue residue hemostatic dressing with superior performance in bleeding control. Loading of drugs in these clay nanotubes following with their sustain release opens further perspective for this formulation development.

## 4. Experimental Section

*Materials*: HNTs (mined from Hebei Province, China) were obtained from Guangzhou Runwo Materials Technology Co., Ltd., China. Alginate and $CaCl_2$ were bought from Macklin-reagent Inc., China. Cotton

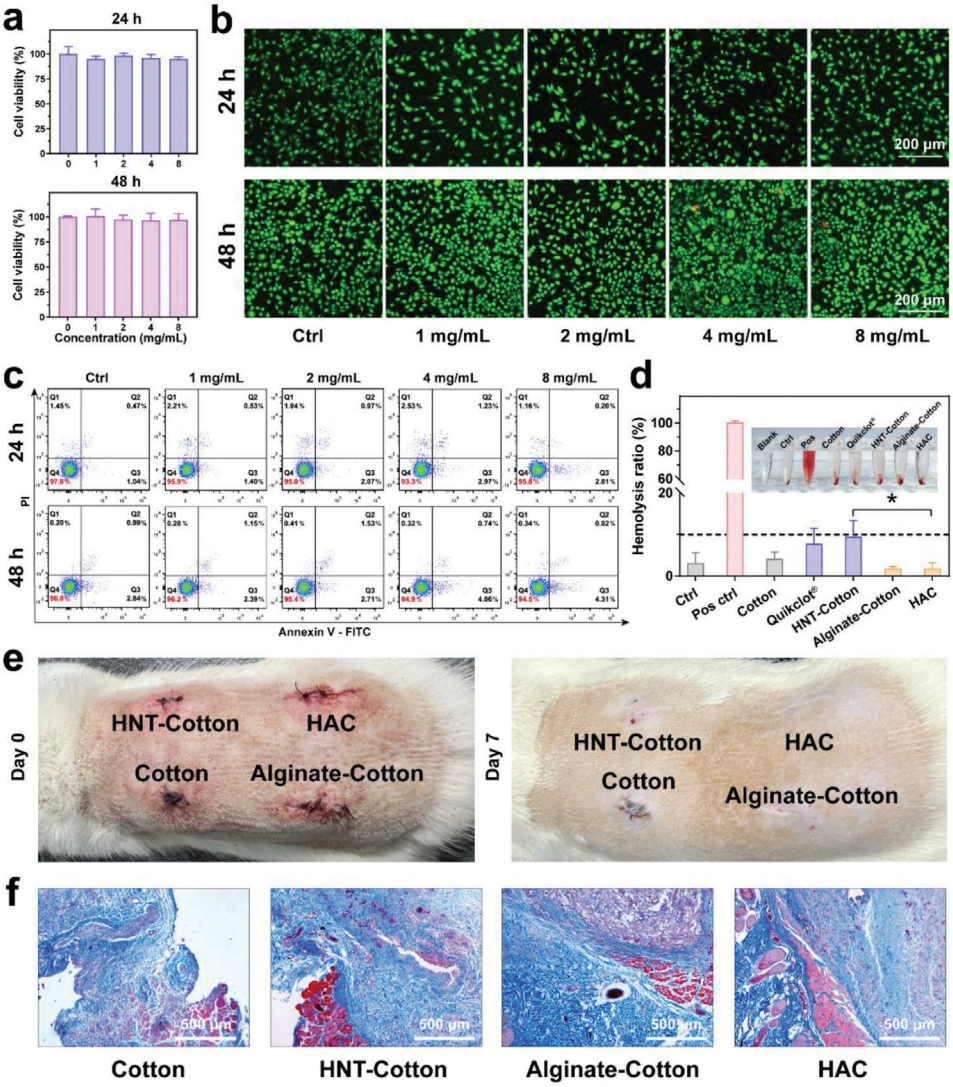


**Figure 8.** Biocompatibility assay. Cytotoxicity of gradient concentration of HAC tested via a) CCK-8 assay, b) calcein AM/prodium iodide live/dead staining, and c) apoptosis and necrosis analysis. d) Hemolysis ratio of cotton, QuikClot combat gauze, HNT-Cotton, Alginate-Cotton, and HAC. e) Photograph for the wound regions in rat back implant experiment. Wounds were implanted with cotton, HNT-Cotton, Alginate-Cotton, and HAC fabrics immediately following surgery (day 0) and for 7 days. f) Tissue Masson staining of implantation site on day 7. $*p < 0.05$, and data are presented as mean ± SD.

non-woven fabric fibers (MRJ426-3, Zhejiang Grace Group, China) and QuikClot combat gauze (Z-Medica, USA) was purchased from commercial sources. CD41-FITC and CD62p-Phycoerythrin antibodies were bought from BD Biosciences Inc., USA. Other clays were bought from Macklin-reagent Inc., China. Cell culture-related reagents were obtained from Thermo Fisher Scientific Inc., USA.

*Preparation of HAC*: Non-woven cotton fabrics were chosen as substrates. The fabrics were first immersed in $CaCl_2$ solution (20 mM) and dried to obtain $Ca^{2+}$-rich fibers. Then, the HNTs were assembled on the fibers by capillary effect in a well-dispersed aqueous suspension of HNT-alginate. After the water evaporated completely, a robust coating of HNT-alginate on the fibers (named HAC) was obtained. The assembly of HNTs on other medical dressings and fibers followed the method described above.

*Characterization*: The microstructure of HNT-alginate was observed with a TEM (JEM, 1400 Flash). The surface morphology of HAC was observed using SEM (ULTRA55, Carl Zeiss Jena Co. Ltd., Germany) after sputter-coating with a thin film of gold. FTIR spectra of HNT-alginate and HAC were characterized by a FTIR instrument (Nicolet iS50, Thermo Fisher Scientific Inc., USA) ranging from 4000 to 400 $cm^{-1}$. The zeta potential was analyzed using a Nano ZS zeta potential analyzer (Malvern Instruments Co., UK). The XRD patterns of HNT-alginate and modified fabrics were obtained on an X-ray diffractometer (MiniFlex-600, Rigaku Corporation, Japan) with a scan rate of 5 ° $min^{-1}$ and a range of 5–80°. The content of HNTs and alginate in the modified dressings were analyzed on a TGA2 instrument (STAR System, Mettler Toledo Co. Ltd., Switzerland), which ranged from 30 to 700 °C with 10 °C $min^{-1}$ rate of rising. DTG curves were obtained by first-order derivation of the corresponding TGA curves. The rheological behavior of blood with the increase of alginate was tested by a rotating rheometer (Kinexus pro, Malvern Instruments Ltd., UK). TEG analyses were detected by an automated TEG testing system (Haema TX, Shenzhen MedCaptain Medical Technology Co., China).

*Water/Blood Absorption and Water Vapor Transmission Capacity Test*: The pre-weighed dressings were placed in water or blood and weighed

 

immediately after saturation of the absorbent solution. Three tests were performed for each group. Liquid absorption capacity was expressed by a fold change in mass. The formula was as follows:

$$\text{Fold change} = \frac{\text{weight}_{\text{liquid}}}{\text{weight}_{\text{material}}} \quad (1)$$

For measuring water vapor permeability, a glass bottle containing 20 mL of distilled water was covered with the dressing. The mouth of the bottle was tightly sealed to avoid water vapor loss through the boundary. The weight of the entire system was measured at the specified time point at 60 °C. Photos were taken by covering the dressing with a humidifier.

*In Vivo Fluorescence Imaging*: HNTs (100 mg) were labeled with FITC (1 mg $mL^{-1}$) at 4 °C for 24 h and washed with water to obtain HNT-FITC. FITC-HAC was also prepared with a similar method. Kaolin of QuikClot combat gauze was collected by washing with water, labeled with FITC, and dropped back onto the original gauze to obtain FITC-QuikClot combat gauze. KM female mice (8 weeks old, 25–30 g) were purchased from the Laboratory Animal Center of Southern Medical University. This study followed the Guide for the Care and Use of Laboratory Animals and complied with animal welfare guidelines. Ethical approval for this study was received from Guangzhou Huawei Testing Co., Ltd., China (approval number: HWT-BG-117). Mice were anesthetized, and a 2 × 2 $cm^2$ full-length wound was placed on the back of the mice. The wound was treated with dressings, and the peel-offed clay powder in the wound was observed using in vivo fluorescence system (IVIS spectroscopy, excitation: 480 nm, emission: 520 nm). Ultimately, all mice were euthanized with the cervical dislocation method.

*Blood Coagulation In Vitro*: Clotting assays were performed using sodium citrate sheep whole blood. Samples (2 mg) were added to the tubes; samples included blank control, cotton, $Ca^{2+}$-Cotton, QuikClot combat gauze, HNT-Cotton, Alginate-Cotton, and HAC. 1 mL of blood was added and incubated with the samples for 5 min, followed by the addition of 100 µL of 0.2 M $CaCl_2$ to trigger clotting. The blood was shaken in a 37 °C water bath till it was utterly clotted, and the duration was recorded as the clotting time. A similar method was also used to evaluate the coagulation capacity of $Ca^{2+}$ or alginate alone.

To compare clotting rates, 100 µL of recalcified blood (0.2 M $CaCl_2$ to blood ratio: 1:10) was dropped into each sample, and the samples were clotted at 37 °C for 0, 2, 4, 5, and 6 min, followed by the gentle addition of 1 mL of water to abort the reaction without disturbing the clot. Finally, the absorbance of the supernatant was tested at 540 nm, reflecting the release of hemoglobin (HA) from free erythrocytes. The unclotted state was indicated at 0 min. Relative HA (RHA) was calculated by the following formula. A higher RHA indicated a slower clotting rate.

$$\text{RHA}\ (\%) = \frac{\text{HA}\,(t)}{\text{HA}\,(0)} \times 100\% \quad (2)$$

In addition, the interaction of HAC with blood cells was studied by SEM. 50 µL of recalcified whole blood was dropped onto a 1 $cm^2$ sample and incubated for 5 min at 37 °C. Samples were fixed with 2.5% glutaraldehyde for 2 h. Then, the samples were washed twice with PBS and dehydrated with 30%, 50%, 70%, 80%, 90%, and 100% (twice) ethanol (30 min for each step). After supercritical $CO_2$ drying, SEM was used to observe blood cells' adsorption, activation, and clotting.

Flow cytometry was used to quantify platelet activation. HAC (1, 2, or 4 mg) was placed in tubes and mixed with 90 µL of whole blood for 5 min. Untreated whole blood was used as a control, and 10 mM collagen solution was used as a positive control. Treated blood was stained with antibodies (CD41-FITC and CD62p-phycoerythrin) for 20 min. At last, the data were tested by flow cytometry (Canto, BD Biosciences, USA) and analyzed using FlowJo 10.0.2 software (BD Biosciences, USA).

*In Vivo Hemostasis Test in the Rat Model*: All experimental procedures in this study were performed following the appropriate ethical guidelines, and the use of animals in this study was approved by the Management Committee of the Medical Laboratory Animal Center of Jinan University (approval number: 20220506-07). A rat liver hemorrhage model (Sprague-Dawley rats, 350–400 g, males) was used to evaluate the effects of different hemostatic dressings. Rats were anesthetized using a 4% sodium barbiturate solution (40 mg $kg^{-1}$). An abdominal incision was made to expose the rat's liver, and pre-weighed filter paper was placed underneath the liver. A piece of liver (2 cm × 5 mm × 5 mm) was cut off to cause bleeding, and about 500 mg of pre-weighed hemostatic dressing was applied to the wound to stop bleeding. The amount of blood loss was calculated from the final weight of the filter paper and dressing, and the total duration of hemostasis was recorded. The temperature change of the wound during hemostasis was detected by infrared thermometry. Each group used five rats.

To further test the ability of several dressings to control massive bleeding, a rat model of hemorrhage from ruptured femoral arteries and veins was used. Immediately after the vessel rupture, two to three pre-weighed dressings were applied to stop the bleeding. The amount of blood loss and the time and temperature of hemostasis were recorded. Five rats were used in each group.

*Biocompatibility Evaluation*: L929 fibroblasts were used for cytotoxicity evaluation. Cells were cultured in Dulbecco's Modified Eagle Medium with 10% fetal bovine serum and maintained at 37 °C and 5% $CO_2$. The leachate (per 10 mg in 1 mL of medium, defined as 100%) was obtained by immersing autoclaved HAC in the medium for 24 h. Gradient dilutions were made to obtain 0% and 20, 40, 60, 80, or 100% extracts for subsequent testing. CCK-8 assay was used for cell viability assessment. Cells in the logarithmic growth phase were inoculated in 96-well plates and treated with HAC leachate. After 24 or 48 h, 10 µL of CCK-8 solution was added to each well and incubated at 37 °C for 4 h. Afterward, the absorbance at 450 nm was measured using a microplate reader (Elx800, Bio-Tek, USA). Each experiment was performed 3 times.

Morphological evidence of dead/live cells was analyzed using calcein AM/prodium iodide live/dead staining. L929 cells (3 × $10^4$ $mL^{-1}$) were inoculated in 24-well plates and treated with leachate for 24 or 48 h. After staining was done according to the instructions, cells were observed under a fluorescent microscope (Axio Vert. A1, Zeiss, Germany), and images were taken in a random field of view.

Cell culture for flow cytometry was conducted as above. Cells were digested with trypsin and collected at a certain time point. Cells were dispersed in 400 µL buffer and stained with 5 µL Annexin V-FITC antibody and 10 µL propidium iodide for 15 min and then assayed using a flow cytometer (Canto, BD Biosciences, USA). The results were analyzed by FlowJo 10.0.2 (BD Biosciences, USA).

Hemolysis experiments were performed using sodium citrate sheep blood. The erythrocytes were washed 3 times with PBS to remove the background HA. Erythrocytes were diluted tenfold, and 200 µL was added to each sample solution (5 mg of sample was added to 800 µL of PBS). Ultrapure water (+erythrocytes) and PBS (+erythrocytes) were positive and blank controls. All samples were incubated for 2 h at 37 °C. The samples were centrifuged at 1000 × *g* for 5 min to precipitate the erythrocytes, while the broken erythrocytes released the HA in the supernatant. The absorbance at 540 nm was measured using a microplate reader (Elx800, BioTek, USA). The hemolysis rate was calculated as follows:

$$\text{Hemolysis rate}\ (\%) = \frac{\text{OD}_{\text{Sample}} - \text{OD}_{\text{Blank}}}{\text{OD}_{\text{Positive}} - \text{OD}_{\text{Blank}}} \times 100\% \quad (3)$$

To assess the biocompatibility of the materials in vivo, Sprague–Dawley rats were anesthetized with sodium pentobarbital, and subcutaneous incisions were created in the dorsal skin after removing the dorsal hair. Each group's material (10 mg) was embedded subcutaneously, immediately sutured, and disinfected with an iodophor. The skin reaction of each group was observed on day 7, and the rats were executed. The tissue samples were fixed in 4% paraformaldehyde and then submitted to Wuhan Servicebio Technology Co., Ltd. for histological processing and Masson trichrome staining. Representative images of each group were shown in the corresponding figures.

*Statistical Analysis*: All data were shown as means ± SD via at least triplicate samples. Statistically significant differences between groups were analyzed by two-tailed *t*-tests with GraphPad Prism 7 (GraphPad Software, USA), and a two-sided *p*-value < 0.05 was considered statistically significant. Two or more groups were compared separately by one-way ANOVA (analysis of variance) using a Tukey post-hoc analysis.

## Supporting Information

Supporting Information is available from the Wiley Online Library or from the author.

## Acknowledgements

The authors acknowledge the financial support received from the National Natural Science Foundation of China (52073121), Natural Science Foundation of Guangdong Province (2019A1515011509), Science and Technology Planning Project of Guangzhou (202102010117), and the Fundamental Research Funds for the Central Universities (21622406). Y.L. thanks support by Louisiana Board of Regent grant LEQSF (2020-21)-RD-D-03.

## Conflict of Interest

The authors declare no conflict of interest.

## Data Availability Statement

The data that support the findings of this study are available from the corresponding author upon reasonable request.

## Keywords

alginate, assembly, clay, dressing, hemostasis, nanotube

Received: September 5, 2022
Revised: October 20, 2022
Published online: November 10, 2022

[1] J. W. Cannon, *N. Engl. J. Med.* **2018**, *378*, 370.
[2] M. Long, Y. Zhang, P. Huang, S. Chang, Y. H. Hu, Q. Yang, L. F. Mao, H. M. Yang, *Adv. Funct. Mater.* **2018**, *28*, 1704452.
[3] H. He, W. Zhou, J. Gao, F. Wang, S. Wang, Y. Fang, Y. Gao, W. Chen, W. Zhang, Y. Weng, Z. Wang, H. Liu, *Nat. Commun.* **2022**, *13*, 552.
[4] L. Yu, X. Shang, H. Chen, L. Xiao, Y. Zhu, J. Fan, *Nat. Commun.* **2019**, *10*, 1932.
[5] a) J. Leonard, J. Zietlow, D. Morris, K. Berns, S. Eyer, K. Martinson, D. Jenkins, S. Zietlow, *J. Trauma Acute Care Surg.* **2016**, *81*, 441; b) B. S. Kheirabadi, J. E. Mace, I. B. Terrazas, C. G. Fedyk, J. S. Estep, M. A. Dubick, L. H. Blackbourne, *J. Trauma* **2010**, *68*, 269.
[6] F. Arnaud, T. Tomori, W. Carr, A. McKeague, K. Teranishi, K. Prusaczyk, R. McCarron, *Ann. Biomed. Eng.* **2008**, *36*, 1708.
[7] G. Li, K. Quan, Y. Liang, T. Li, Q. Yuan, L. Tao, Q. Xie, X. Wang, *ACS Appl. Mater. Interfaces* **2016**, *8*, 35071.
[8] P. Zhao, Y. Feng, Y. Zhou, C. Tan, M. Liu, *Bioact. Mater.* **2023**, *20*, 355.
[9] Y. Cui, Z. Huang, L. Lei, Q. Li, J. Jiang, Q. Zeng, A. Tang, H. Yang, Y. Zhang, *Nat. Commun.* **2021**, *12*, 5922.
[10] B. L. Guo, R. N. Dong, Y. P. Bang, M. Li, *Nat. Rev. Chem.* **2021**, *5*, 773.
[11] G. S. Lee, Y. J. Lee, K. Ha, K. B. Yoon, *Adv. Mater.* **2001**, *13*, 1491.
[12] R. N. Udangawa, P. E. Mikael, C. Mancinelli, C. Chapman, C. F. Willard, T. J. Simmons, R. J. Linhardt, *ACS Appl. Mater. Interfaces* **2019**, *11*, 15447.
[13] Y. Feng, X. Luo, F. Wu, H. Z. Liu, E. Y. Liang, R. R. He, M. X. Liu, *Chem. Eng. J.* **2022**, *428*, 132049.
[14] K. Fakhruddin, R. Hassan, M. U. A. Khan, S. N. Allisha, S. I. Abd Razak, M. H. Zreaqat, H. F. M. Latip, M. N. Jamaludin, A. Hassan, *Arab J. Chem.* **2021**, *14*, 103294.
[15] a) M. Massaro, P. Poma, G. Cavallaro, F. Garcia-Villen, G. Lazzara, M. Notarbartolo, N. Muratore, R. Sanchez-Espejo, C. Viseras Iborra, S. Riela, *Colloids Surf., B* **2022**, *213*, 112385; b) M. Massaro, A. Borrego-Sanchez, R. Sanchez-Espejo, C. V. Iborra, G. Cavallaro, F. Garcia-Villen, S. Guernelli, G. Lazzara, D. Miele, C. I. Sainz-Diaz, G. Sandri, S. Riela, *Appl. Clay Sci.* **2021**, *215*, 215.
[16] M. Massaro, E. Licandro, S. Cauteruccio, G. Lazzara, L. F. Liotta, M. Notarbartolo, F. M. Raymo, R. Sanchez-Espejo, C. Viseras-Iborra, S. Riela, *J. Colloid Interface Sci.* **2022**, *620*, 221.
[17] M. Long, B. Zhang, S. Y. Peng, J. Liao, Y. Zhang, J. Wang, M. Wang, B. Qin, J. F. Huang, J. Huang, X. P. Chen, H. M. Yang, *Mater. Sci. Eng., C* **2019**, *105*, 110081.
[18] Y. Zhao, E. Abdullayev, Y. Lvov, presented at *IOP Conference Series: Materials Science and Engineering*, XX, Madrid August, **2014**.
[19] Y. Zhao, E. Abdullayev, A. Vasiliev, Y. Lvov, *J. Colloid Interface Sci.* **2013**, *406*, 121.
[20] D. Tunega, A. Zaoui, *J. Phys. Chem. C* **2020**, *124*, 7432.
[21] A. Panchal, G. Fakhrullina, R. Fakhrullin, Y. Lvov, *Nanoscale* **2018**, *10*, 18205.
[22] C. Li, C. Lan, M. Guo, N. Wang, Y. Ma, *Langmuir* **2020**, *36*, 13963.
[23] A. Skogberg, S. Siljander, A. J. Maki, M. Honkanen, A. Efimov, M. Hannula, P. Lahtinen, S. Tuukkanen, T. Bjorkqvist, P. Kallio, *Nanoscale* **2022**, *14*, 448.
[24] X. Huang, J. X. He, K. Sun, Y. F. Chen, Z. G. Zha, C. R. Zhou, *Carbon* **2018**, *129*, 258.
[25] H. Li, J. Zhao, L. Huang, P. Xia, Y. Zhou, J. Wang, L. Jiang, *ACS Nano* **2022**, *16*, 6224.
[26] C. Lan, M. Guo, C. Li, Y. Qiu, Y. Ma, J. Sun, *ACS Appl. Mater. Interfaces* **2020**, *12*, 7477.
[27] X. Liang, H. Li, J. Dou, Q. Wang, W. He, C. Wang, D. Li, J. M. Lin, Y. Zhang, *Adv. Mater.* **2020**, *32*, 2000165.
[28] X. Zhao, W. Gao, W. Yao, Y. Jiang, Z. Xu, C. Gao, *ACS Nano* **2017**, *11*, 9663.
[29] B. Furie, B. C. Furie, *Cell* **1988**, *53*, 505.
[30] L. A. Zhao, G. X. You, F. L. Liao, X. M. Kan, B. Wang, Q. M. Sun, H. B. Xu, D. Han, H. Zhou, *Artif. Cells, Blood Substitutes, Biotechnol.* **2010**, *38*, 267.
[31] M. Liu, R. Fakhrullin, A. Novikov, A. Panchal, Y. Lvov, *Macromol. Biosci.* **2019**, *19*, 1800419.
[32] M. Kohno, Y. Nara, M. Kato, T. Nishimura, *Clay Miner.* **2018**, *53*, 721.
[33] V. J. Bom, R. M. Bertina, *Biochem. J.* **1990**, *265*, 327.
[34] M. Liu, R. He, J. Yang, W. Zhao, C. Zhou, *ACS Appl. Mater. Interfaces* **2016**, *8*, 7709.
[35] M. Tharmavaram, G. Pandey, D. Rawtani, *Adv. Colloid Interface Sci.* **2018**, *261*, 82.
[36] Y. Lvov, W. Wang, L. Zhang, R. Fakhrullin, *Adv. Mater.* **2016**, *28*, 1227.
[37] A. Hasan, P. Fatehi, *Appl. Clay Sci.* **2018**, *158*, 72.
[38] M. Du, B. Guo, Y. Lei, M. Liu, D. Jia, *Polymer* **2008**, *49*, 4871.
[39] E. Magovac, B. Voncina, I. Jordanov, J. C. Grunlan, S. Bischof, *Materials (Basel)* **2022**, *15*, 432.
[40] a) E. H. Portella, D. Romanzini, C. C. Angrizani, S. C. Amico, A. J. Zattera, *Mater. Res.* **2016**, *19*, 542; b) Z. Y. Huang, P. Wu, Y. K. Yin, X. Zhou, L. Fu, L. X. Wang, S. H. Chen, X. Tang, *Cellulose* **2021**, *28*, 11037.

[41] B. M. M. Baharoon, A. M. Shaik, S. M. El-Hamidy, R. E. El-Araby, A. H. Batawi, M. A. Salam, *Saudi J. Biol. Sci.* **2022**, *29*, 3626.
[42] K. Ramadass, G. Singh, K. S. Lakhi, M. R. Benzigar, J. H. Yang, S. Kim, A. M. Almajid, T. Belperio, A. Vinu, *Microporous Mesoporous Mater.* **2019**, *277*, 229.
[43] P. X. Zhao, Y. Feng, Y. Q. Zhou, C. Y. Tan, M. X. Liu, *Bioact. Mater.* **2023**, *20*, 355.
[44] T. T. Chau, W. J. Bruckard, P. T. L. Koh, A. V. Nguyen, *Adv. Colloid Interface Sci.* **2009**, *150*, 106.
[45] A. Hawreen, J. A. Bogas, *Adv. Civ. Eng. Mater.* **2019**, *8*, 307.
[46] L. Bacakova, M. Vandrovcova, I. Kopova, I. Jirka, *Biomater. Sci.* **2018**, *6*, 974.
[47] D. J. Lim, I. Jang, *Polymers* **2021**, *13*, 4131.
[48] S. Pourshahrestani, E. Zeimaran, I. Djordjevic, N. A. Kadri, M. R. Towler, *Mater. Sci. Eng., C* **2016**, *58*, 1255.
[49] J. H. Griffin, *Proc. Natl. Acad. Sci. USA* **1978**, *75*, 1998.
[50] H. L. Zhang, *Nanotechnol. Rev.* **2017**, *6*, 573.
[51] a) T. W. Zhang, J. Zhao, X. Y. Lv, F. Liu, X. L. Wang, K. Li, Z. Y. Bai, H. Y. Chen, W. Q. Tian, *J. Nanopart. Res.* **2021**, *23*, 240; b) Z. Li, B. L. Li, X. R. Li, Z. F. Lin, L. L. Chen, H. Chen, Y. Jin, T. Zhang, H. Xia, Y. Lu, Y. Zhang, *Carbohydr. Polym.* **2021**, *267*, 118155.
[52] A. C. Santos, I. Pereira, S. Reis, F. Veiga, M. Saleh, Y. Lvov, E. Opin, *Drug Delivery* **2019**, *16*, 1169.
[53] H. T. Peng, *Mil. Med. Res.* **2020**, *7*, 13.
[54] R. Narayan, *Encyclopedia of Biomaterials and Biomedical Engineering*, Elsevier, Amsterdam, Holland **2019**.